Neuro-Oncology 15(10):1317–1329, 2013.
doi:10.1093/neuonc/not084
Advance Access publication June 27, 2013

NEURO-ONCOLOGY

Cooperativity between MAPK and PI3K signaling activation is required for glioblastoma pathogenesis

Mark Vitucci‡, Natalie O. Karpinich‡, Ryan E. Bash, Andrea M. Werneke, Ralf S. Schmid, Kristen K. White, Robert S. McNeill, Byron Huff, Sophie Wang, Terry Van Dyke, and C. Ryan Miller

Curriculum in Genetics and Molecular Biology (M.V.), Department of Cellular and Molecular Physiology (N.O.K.), Division of Neuropathology, Department of Pathology and Laboratory Medicine (R.E.B., A.M.W., R.S.M., B.H., C.R.M.), Program in Molecular Biology and Biotechnology (R.S.S., C.R.M.), Lineberger Comprehensive Cancer Center (R.S.S., K.K.W., C.R.M.), Department of Neurology and Neurosciences Center, University of North Carolina School of Medicine, Chapel Hill, North Carolina (C.R.M.); and Mouse Cancer Genetics Program (S.W., T.V.D.) and Center for Advanced Preclinical Research (T.V.D.), NCI-Frederick, Frederick, Maryland

Background. Glioblastoma (GBM) genomes feature recurrent genetic alterations that dysregulate core intracellular signaling pathways, including the G1/S cell cycle checkpoint and the MAPK and PI3K effector arms of receptor tyrosine kinase (RTK) signaling. Elucidation of the phenotypic consequences of activated RTK effectors is required for the design of effective therapeutic and diagnostic strategies.

Methods. Genetically defined, G1/S checkpoint-defective cortical murine astrocytes with constitutively active Kras and/or Pten deletion mutations were used to systematically investigate the individual and combined roles of these 2 RTK signaling effectors in phenotypic hallmarks of glioblastoma pathogenesis, including growth, migration, and invasion in vitro. A novel syngeneic orthotopic allograft model system was used to examine in vivo tumorigenesis.

Results. Constitutively active Kras and/or Pten deletion mutations activated both MAPK and PI3K signaling. Their combination led to maximal growth, migration, and invasion of G1/S-defective astrocytes in vitro and produced progenitor-like transcriptomal profiles that mimic human proneural GBM. Activation of both RTK effector arms was required for in vivo tumorigenesis and produced highly invasive, proneural-like GBM.

Conclusions. These results suggest that cortical astrocytes can be transformed into GBM and that combined dysregulation of MAPK and PI3K signaling revert G1/S-defective astrocytes to a primitive gene expression state. This genetically-defined, immunocompetent model of proneural GBM will be useful for preclinical development of MAPK/PI3K-targeted, subtype-specific therapies.

Keywords: astrocytes, genetically engineered mouse, glioblastoma, invasion, Pten.

Glioblastomas (GBM; World Health Organization [WHO] grade IV) account for >85% of astrocytomas and are uniformly lethal.[1] Their diffuse infiltration of normal brain makes complete surgical resection impossible, and further eradicating tumor cells with radiation or chemotherapy remains difficult. Thus, recurrence is almost certain, occurring in at least 90% of cases near the resection site.[2,3] This sobering clinical reality has fueled investigation of the biological mechanisms responsible for GBM migration and invasion, particularly the intracellular signaling pathways that govern these phenotypes. The Cancer Genome Atlas (TCGA) catalogued oncogenic mutations and copy number alterations in GBM and showed that these abnormalities occur primarily in genes of 3 core intracellular pathways, namely the RB-regulated G1/S cell cycle checkpoint, receptor tyrosine kinase (RTK) signaling, and TP53. Approximately 74% of human GBM harbored events in all 3 pathways, whereas <5% harbored events in only one of the three.[4] In contrast, over 90% contained

Received November 26, 2012; accepted April 28, 2013.

‡These authors contributed equally to this work.

Corresponding Author: C. Ryan Miller, MD, PhD, University of North Carolina School of Medicine, 6109B Neurosciences Research Building, Campus Box 7250, Chapel Hill, NC 27599–7250 (rmiller@med.unc.edu).

mutations in both RB and RTK pathway genes (http://tcga-data.nci.nih.gov/tcga/).

RTK and their downstream effectors, RAS/MAPK and PI3K/AKT/mTOR, have received particular interest, because kinases within these pathways represent potential targets for therapeutic intervention.[5] RTK pathway kinases encoded by the *EGFR*, *ERBB2*, *PDGFRA*, *MET*, *KRAS*, *PIK3CA*, and *AKT1* genes are frequently amplified or mutationally activated, whereas negative regulators of RAS and PI3K signaling, *NF1* and *PTEN*, are frequently deleted or mutationally inactivated, respectively.[4] On the basis of these genetic alterations, 88% of GBM are predicted to harbor activated RTK signaling through these 2 effector arms, and virtually all show RAS activation.[6,7]

However, clinical trial results with RTK-targeted therapeutics, particularly EGFR tyrosine kinase inhibitors (TKI), have been disappointing.[8] *EGFR* is amplified or mutated in 36%–45% of GBM,[4,9] but only a small percentage of these tumors respond to EGFR TKI. GBM exhibit both inter- and intratumoral genetic heterogeneity, and both neighboring and individual tumor cells can harbor amplifications in >1 distinct RTK gene.[10] A recent mouse model study showed that Met may functionally compensate for EGFR signaling after EGFR TKI-mediated inhibition, suggesting one potential resistance mechanism particularly in the subset of GBM with *EGFR* and *MET* coamplification.[11] In addition, coexpression of the constitutively active EGFRvIII extracellular domain truncation mutant and PTEN correlated with EGFR TKI response. In contrast, loss of PTEN expression was associated with treatment failure, suggesting that uncoupling of PI3K signaling from EGFR may be an additional EGFR TKI resistance mechanism.[12]

Since its discovery >10 years ago, the *PTEN* tumor suppressor gene has been extensively investigated. The embryonic lethality observed in *Pten*-null mice underscores its importance during development.[13,14] *PTEN* is also critical in many cellular functions relevant to tumorigenesis, including proliferation, survival, migration, and invasion.[15] Inactivating *PTEN* mutations or deletions are present in 30%–40% of human GBM, and TCGA identified it as the second most commonly mutated GBM gene.[4,16] A more complete understanding of the combinatorial roles of RTK signaling through RAS and PI3K effectors in GBM pathogenesis, particularly the migratory and invasive phenotypes that make treatment difficult, is therefore required to develop more effective, targeted therapies.[3]

To overcome this limitation, we have generated primary astrocytes from a series of conditional, genetically engineered mouse (GEM) models, in which 2 of the 3 core GBM pathways were genetically targeted, either alone or in combination, all on a common C57Bl/6-based genetic background. After Cre-mediated recombination, these mice express an N-terminal 121-amino acid truncation mutant of SV40 large T antigen (T_{121}, hereafter called T) from the human glial fibrillary acidic protein (GFAP) promoter,[17] which inactivates all 3 Rb family proteins—Rb, p107, and p130—and ablates the G1/S cell cycle checkpoint.[18] In addition, these mice have a constitutively active $Kras^{G12D}$ mutant (R)[19] and/or either heterozygous or homozygous *Pten* deletion ($P^{+/-}$ or $P^{-/-}$).[20] Our previous studies have shown that particular combinations of these 3 alleles recapitulate the histopathological progression from low-grade (WHO grade II, A2) to high-grade astrocytomas (WHO grade III and IV, A3 and GBM, respectively) after recombination in adult $GFAP^{+}$ mouse brain cells.[20] Therefore, we hypothesized that these primary GEM astrocytes would provide a unique opportunity to dissect the individual and combinatorial roles of activated MAPK and PI3K signaling in biological processes relevant to GBM pathogenesis, including cellular growth (proliferation and apoptosis), migration, and invasion in vitro and tumorigenesis in vivo.

Materials and Methods

Genetically Engineered Mice

Heterozygous $TgGZT_{121}$ mice were maintained on a BDF1 background.[17] Heterozygous $Kras^{G12D}$ conditional knock-in and $Pten^{loxP/loxP}$ mice were maintained on a C57/Bl6 background.[19,21] All experimental animals were >94% C57/Bl6. PCR genotyping was performed as previously described.[17,19,21] Animal studies were approved by the University of North Carolina Institutional Animal Care and Use Committee.

Primary Astrocyte Cultures

Primary astrocytes were cultured as previously described.[17] In brief, cells were selectively harvested from the cortices of postnatal day 1–4 pups, manually dissociated by trituration in trypsin, and incubated at 37°C for 20 min. Cells were pelleted, resuspended, and cultured in DMEM supplemented with 10% fetal bovine serum and 1% penicillin–streptomycin (complete media). At 50% confluence, cells were infected at a multiplicity of infection of 50 for 6 h in complete media with a recombinant adenoviral vector expressing Cre recombinase from the constitutive cytomegalovirus promoter (Ad5CMVCre, University of Iowa Gene Transfer Vector Core).[22] After infection, cells were rinsed in phosphate-buffered saline and cultured in complete media at 37°C in 5% CO_2. All immunoblot, cell growth, apoptosis, wound closure, collagen invasion, time-lapse microscopy, microarray, and orthotopic allograft experiments were performed with genotype-confirmed primary astrocytes, under passage 10 post-Ad5CMVCre infection, in log phase growth, and cultured in complete media unless otherwise stated.

Microarray Analyses

All original microarray data are publically available at the UNC Microarray Database (http://genome.unc.edu) and Gene Expression Omnibus, accession number GSE40265.

Orthotopic Allografts

Adult wild-type C57Bl/6 mice ($\geq$ 3 months of age) were anesthetized with Avertin (250 mg/kg) and placed in a stereotactic frame (Kopf, Tujunga, CA). After a 0.5-cm scalp incision, 10^5 cells in 5 μL of 5% methylcellulose were injected into the right basal ganglia using coordinates 1, -2, and -4 mm (A, L, D) from the Bregma suture as previously described.[23]

Statistics

Apoptosis, viability, and time-lapse microscopy data were analyzed using 1-way ANOVA with Tukey's multiple comparisons correction in GraphPad Prism 5 (GraphPad, San Diego, CA). Wound closure data were analyzed using pairwise Student's *t* tests. Doubling times from cell growth assays were compared using 1-way ANOVA with Tukey's correction in Stata, version 10 (College Station, TX). Multiple linear regression, Kaplan–Meier plots, and log-rank analyses were conducted in Stata. All comparisons were significant at $\alpha = 0.05$.

Supplement

Supplemental methods, figures, tables, and videos can be found online.

Results

PI3K and MAPK Signaling and Growth of G1/S Checkpoint-Defective Primary Astrocytes

To determine how targeted genetic disruption of Rb, Ras, and PI3K signaling affects tumorigenesis, we isolated and cultured primary cortical astrocytes from newborn mouse pups with the following genotypes: T, TR, $TP^{wt/loxP}$, $TP^{loxP/loxP}$, $TRP^{wt/loxP}$, and $TRP^{loxP/loxP}$. After infection with Ad5CMVCre to induce recombination, we performed a series of in vitro experiments to probe how these genetic events affect PI3K and Ras/MAPK signaling, proliferation, apoptosis, migration, invasion, and gene expression.

The Rb family of G1/S cell cycle checkpoint regulatory proteins Rb1, p107, and p130 are encoded in mice by *Rb1*, *Rbl1*, and *Rbl2*. Deletion of all 3 Rb family genes in mouse embryonic fibroblasts disrupts this checkpoint and enhances cell cycle entry.[18] We confirmed that T-mediated inactivation of all 3 Rb family proteins disrupted the G1/S checkpoint because T but not wild-type astrocytes continued to enter S phase and proliferate after serum starvation in media with 0.5% serum (data not shown). Under normal growth conditions, T astrocytes showed essentially no activation of the PI3K pathway effectors Akt and S6 (Fig. 1A). Moreover, p-Akt and p-S6 levels were similar to wild-type astrocytes (Supplementary Fig. S1A). These results demonstrate that a defective G1/S checkpoint alone does not activate PI3K signaling (Fig. 1A). *Pten* deletion ($TP^{+/-}$ and $TP^{-/-}$) increased PI3K pathway activation, because p-Akt and p-S6 levels in $TP^{-/-} >> TP^{+/-} >$ T astrocytes. Kras activation (TR and $TRP^{+/-}$) further increased Akt and S6 phosphorylation. Akt and S6 phosphoprotein levels in at least 2 of 3 TR and $TRP^{+/-}$ isolates were similar to astrocytes completely lacking Pten ($TP^{-/-}$ and $TRP^{-/-}$). These results indicate that activated Kras, biallelic *Pten* deletion, or their combination potentiates PI3K pathway signaling in G1/S-defective astrocytes.

We also measured MAPK pathway activation. In at least 2 of 3 isolates per genotype, p-Mek1/2 levels were $TRP^{-/-} > TRP^{+/-} > TP^{-/-} >$ TR $\geq TP^{+/-} \geq$ T $\geq$ wild-type astrocytes (Fig. 1A and Supplementary Fig. S1A). These data suggest that Kras activation (TR) or *Pten* deletion ($TP^{+/-}$, $TP^{-/-}$) alone induce increased MAPK signaling, which is augmented when these mutations are combined ($TRP^{+/-}$, $TRP^{-/-}$). Maximum signaling in $TRP^{-/-}$ astrocytes highlights the combinatorial effects of these mutations on the 2 main RTK effector pathways.

To determine how Rb, Ras, and/or PI3K pathway alterations affected cellular growth, cultured astrocytes from all 6 genotype combinations were counted over 7 days and apoptosis was quantified. Wild-type astrocyte numbers were essentially unchanged throughout the time course examined (Fig. 1B). T astrocytes showed an increased growth rate (5.7 day doubling time) (Fig. 1B and C) and ~2-fold increased apoptosis (Supplementary Fig. S1B) relative to wild-type astrocytes. Similar results were observed in T-driven astrocytomas in vivo.[17] $TP^{+/-}$ and $TP^{-/-}$ astrocytes grew faster (doubling times 4.1 and 3.4 days), and apoptosis in $TP^{-/-}$ was lower than T astrocytes ($P < .05$). Kras activation alone (TR) or in combination with *Pten* deletion ($TRP^{+/-}$, $TRP^{-/-}$) increased growth because TR, $TRP^{+/-}$, and $TRP^{-/-}$ astrocytes displayed the shortest doubling times of 3.8, 3.4, and 2.0 days, respectively (Fig. 1C). Apoptosis levels in TR were lower than T ($P < .05$) but similar to $TP^{-/-}$ astrocytes ($P > .05$) (Fig. 1D and Supplementary Fig. S2), suggesting that the increased growth in $TP^{-/-}$ versus TR astrocytes is attributable to a higher proliferation rate in the former. Apoptosis in $TRP^{-/-}$ astrocytes was lower than both $TP^{-/-}$ and TR ($P < .001$ and $P = .08$, respectively) (Fig. 1D and Supplementary Fig. S2). Overall, these data suggest that activated Kras or Pten loss mitigate the apoptosis induced by T-mediated ablation of the G1/S checkpoint in cultured murine astrocytes. Moreover, the proliferative and anti-apoptotic effects of T, R, and P combined ($TRP^{-/-}$) produced the largest net positive effect on cellular growth.

Both Kras Activation and Pten Loss Contribute to G1/S-Defective Astrocyte Migration In Vitro

We have previously shown that TR, $TRP^{+/-}$, and $TRP^{-/-}$ mice frequently develop high-grade astrocytomas (HGA), including GBM, whereas T, $TP^{+/-}$, and $TP^{-/-}$ mice develop low-grade astrocytomas (LGA) that infrequently progress to HGA.[20] Therefore, we hypothesized that G1/S-defective astrocytes with activated Kras and/or *Pten*

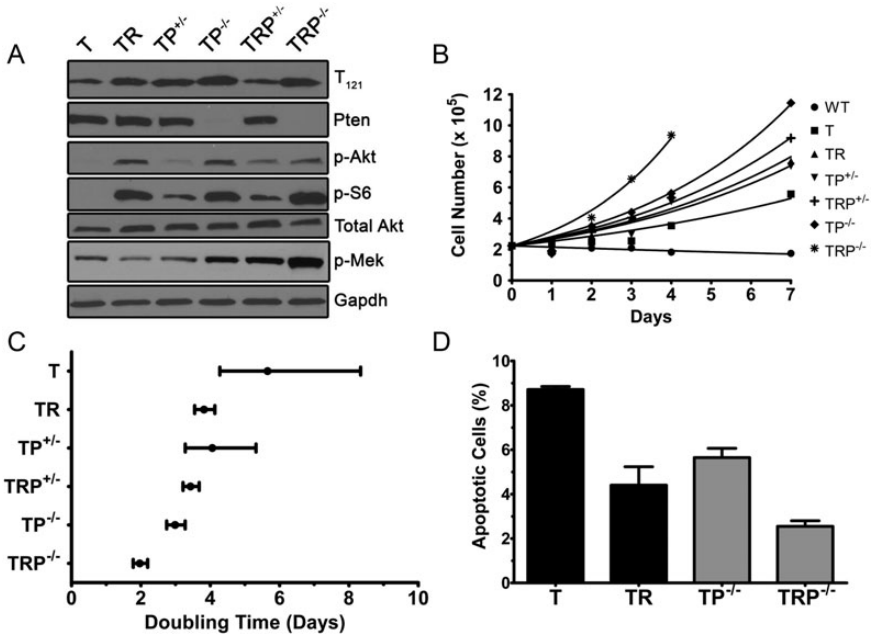

Fig. 1. MAPK and PI3K signaling and growth of G1/S-defective astrocytes with activated Kras and/or Pten deletion. Representative immunoblots showing MAPK and PI3K pathway signaling in G1/S-defective astrocytes with activated Kras, *Pten* deletion, or both (A). Growth of G1/S defective astrocytes in vitro. Cell number was assessed by counting cells at days 1–7 (B). Mean doubling times ± 95% confidence intervals were calculated from the exponential growth curves in B (C). Growth rates were significantly different across genotypes ($P < .0001$). Apoptosis in G1/S defective astrocytes in vitro (D). Colors compare genotypes with and without activated Kras. Error bars represent standard error (SEM).

deletion would display enhanced migration in vitro. To address these hypotheses, we evaluated migration using 2 different assays.

Wound closure, or "scratch," assays have been extensively used to examine the molecular mechanisms of migration.[24] We used this assay to quantify astrocyte migration after 24 h. Activated Kras, alone or in combination with Pten loss, significantly increased migration (Fig. 2A and B) because 2.8-, 2.8-, and 1.9-fold increases in wound closure were evident in TR vs. T, $TRP^{+/-}$ vs. $TP^{+/-}$, and $TRP^{-/-}$ vs. $TP^{-/-}$ astrocytes ($P \leq .0005$). Monoallelic *Pten* deletion did not significantly affect migration of G1/S-defective astrocytes with (TR) and without (T) concomitant Kras activation ($TRP^{+/-}$ vs. TR, $P = .5$; $TP^{+/-}$ vs. T, $P = .6$). In contrast, biallelic *Pten* deletion increased migration by 2.7-fold in $TP^{-/-}$ compared with T astrocytes ($P = .009$), and migration nearly doubled (by 1.8-fold) in $TRP^{-/-}$ compared with TR astrocytes ($P < .0001$). These results show that either Kras activation alone or biallelic Pten deletion, with or without activated Kras, increased G1/S-defective astrocyte migration, and all 3 alterations resulted in maximal migration.

Because wound closure can be achieved through a combination of cell migration, spreading, proliferation, and interaction with neighboring cells, we examined the cell autonomous genetic contributions to migration by tracking cellular movement over 1 h with use of time-lapse video microscopy and calculating the velocities of individual cells (Fig. 2C and videos SV1–4). Wild-type astrocytes were relatively nonmotile. G1/S checkpoint disruption alone (T) increased mean cellular velocity by 4.3-fold compared with wild-type astrocytes. Activated Kras (TR) or *Pten* deletion ($TP^{+/-}$, $TP^{-/-}$) only slightly increased migration of G1/S-defective T astrocytes. TR, $TRP^{+/-}$, and $TRP^{-/-}$ astrocytes migrated faster than their counterparts without activated Kras. Combining all 3 alterations in $TRP^{-/-}$ astrocytes resulted in maximal migration with a mean velocity of 47 ± 2 μm/h. Of note, genotype significantly influenced mean velocity (1-way ANOVA, $P < .0001$), and all pairwise genotype comparisons were significant ($P < .05$) except T vs. $TP^{-/-}$. Multivariable regression analysis confirmed the independent contribution of all 3 alleles ($P < .001$). Taken together, these results showed that Kras activation and/or Pten loss increased G1/S-defective astrocyte migration and that all 3 alterations resulted in maximal migration in both multicellular (Fig. 2B) and individual cell (Fig. 2C) contexts.

We confirmed the effects of activated Ras and PI3K signaling on migration by examining wound closure in $TRP^{-/-}$ astrocytes after pharmacological inhibition of mTOR, PI3K, and MEK with rapamycin, LY294002, and U0126, respectively (Fig. 2D). S6 phosphorylation was virtually eliminated by rapamycin and LY294002 (Supplementary Fig. S6) and decreased wound closure by 22% and 45% ($P \leq .0004$). U0126 inhibited Erk phosphorylation (Supplementary Fig. S3A) and decreased wound closure by 35% ($P < .001$). In contrast, combined inhibition of PI3K and MEK with LY294002

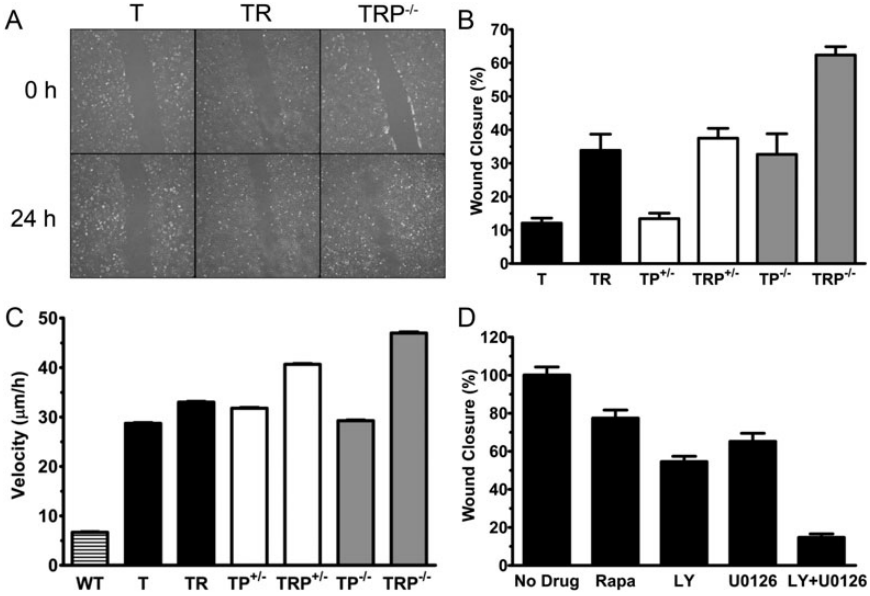

Fig. 2. Kras activation and Pten loss increase G1/S-defective astrocyte migration. Representative photomicrographs of wound closure in T, TR, and $TRP^{-/-}$ astrocytes at 0 and 24 h (A). Mean percent wound closure ± SEM at 24 h (B). Colors compare genotypes with and without activated Kras. Mean velocity ± SEM of individual astrocytes measured using time-lapse microscopy for 1 h (C). Colors compare genotypes with and without activated Kras. Wound closure of $TRP^{-/-}$ astrocytes treated with 10 nM rapamycin (Rapa), 50 μM LY294002 (LY), 10 μM U0126, or both LY294002 and U0126 (D). Mean percent wound closure ± SEM is shown relative to untreated (No Drug) $TRP^{-/-}$ astrocytes.

and U0126 decreased $TRP^{-/-}$ astrocyte wound closure by 85%, relative to untreated $TRP^{-/-}$ astrocytes ($P < .0001$). Moreover, combined LY294002/U0126 treatment decreased $TRP^{-/-}$ astrocyte migration to similar levels as T astrocytes without activated Kras and deleted *Pten* (Fig. 2B) and minimally affected viability at 24 h (data not shown) or 5 days (Supplementary Fig. S3B).

Pten Loss Is Necessary for G1/S-Defective Astrocyte Invasion In Vitro

Astrocytomas are characterized by their ability to invade the surrounding brain parenchyma. We used our astrocyte panel to ascertain which core signaling pathway alterations were necessary for collagen invasion in vitro.[25] T astrocytes showed minimal invasion over 7 days (Fig. 3A and B). Invasion was only 40% higher in TR astrocytes ($P = .6$), suggesting that Kras activation alone was insufficient for invasion. However, a Kras effect was evident when combined with monoallelic *Pten* deletion because $TRP^{+/-}$ showed 19-fold increased invasion compared with $TP^{+/-}$ astrocytes ($P = .01$). In contrast, a Kras-specific effect was not apparent when combined with biallelic *Pten* deletion because $TRP^{-/-}$ showed only a 40% increase in invasion compared with $TP^{-/-}$ astrocytes ($P = .2$). Although monoallelic *Pten* deletion ($TP^{+/-}$) produced a moderate (6-fold), statistically insignificant increase in invasion ($P = .09$), biallelic *Pten* deletion ($TP^{-/-}$) increased invasion by 68-fold compared with T astrocytes ($P < .0001$, Fig. 3B), suggesting that Pten loss alone is sufficient to induce G1/S-defective astrocyte invasion. Deletion of one ($TRP^{+/-}$) or both ($TRP^{-/-}$) *Pten* allele(s) increased invasion by 85- ($P = .01$) and 69-fold ($P = .001$) over G1/S-defective astrocytes with activated Kras (TR). Thus, although the invasion-related effects of Kras activation were evident in G1/S-defective astrocytes with heterozygous, but not homozygous, *Pten* deletion, Pten loss-mediated invasion was independent of Kras activation.

In addition to proliferation and migration, genetic activation of Kras and *Pten* deletion maximally increased G1/S-defective astrocyte invasion in vitro ($TRP^{-/-}$). Therefore, we next confirmed the invasion-related effects of activated PI3K and MEK signaling by examining $TRP^{-/-}$ astrocyte invasion after pharmacological inhibition of mTOR, PI3K, and MEK. Whereas rapamycin, LY294002, and U0126 inhibited $TRP^{-/-}$ astrocyte invasion by 47%, 33%, and 49% ($P > .05$), combined treatment with LY294002/U0126 significantly decreased invasion by 90% ($P = .01$) (Fig. 3C). Of note, all drug treatments minimally affected viability at 5 days ($P > .05$) (Supplementary Fig. S3B).

Pten Restoration Reduces Proliferation, Migration, and Invasion

The data above suggest that PI3K pathway activation induced by Pten loss is critical for G1/S-defective astrocyte proliferation, migration, and invasion. To confirm its role in these processes, we restored Pten expression by infecting $TRP^{-/-}$ astrocytes with a retrovirus encoding wild-type murine *Pten*. Pten expression was evident in ~60% of cells within 48 h of infection and attenuated downstream PI3K signaling at p-Akt (56%–73%) and p-S6 (68%–85%). In contrast, Pten restoration did not

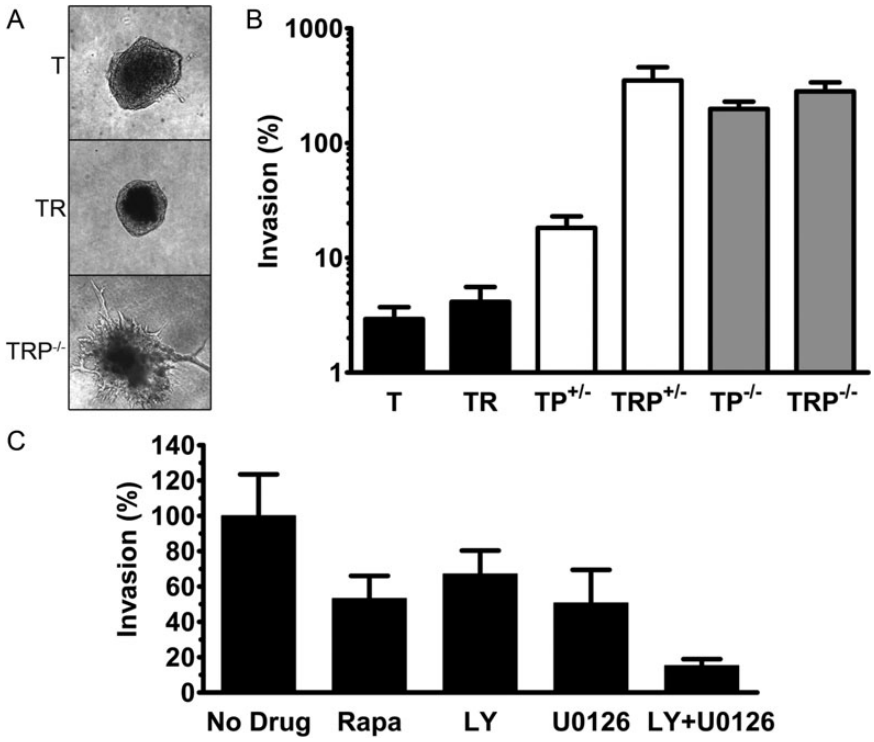

Fig. 3. *Pten* deletion is necessary for maximum G1/S-defective astrocyte invasion. Representative photomicrographs of collagen invasion of T, TR, and $TRP^{-/-}$ astrocytes at 4 days (A). Mean percent invasion ± SEM into collagen after 4 days (B). Colors compare genotypes with and without activated Kras. Collagen invasion of $TRP^{-/-}$ astrocytes treated with 10 nM rapamycin (Rapa), 50 μM LY294002 (LY), 10 μM U0126, or both LY294002 and U0126 (C). Mean percent invasion ± SEM is shown relative to untreated (No Drug) $TRP^{-/-}$ astrocytes.

significantly alter MAPK signaling of p-Mek and p-Erk (Fig. 4A).

Restoring Pten increased $TRP^{-/-}$ astrocyte doubling time from 1.8 to 2.7–3.4 days (Fig. 4B and C), growth rates similar to TR astrocytes without *Pten* deletion (Fig. 1B). Pten also significantly reduced, but did not completely prevent, migration in the wound closure assay ($P \leq .0002$) (Fig. 4D). GFP transfection did not significantly alter migration (Fig. 4D) compared with untransfected $TRP^{-/-}$ astrocytes (Fig. 2B) ($P = .1$). These data are consistent with wound closure (Fig. 2B) and time-lapse microscopy (Fig. 2C) experiments using TR astrocytes and confirm the Kras contribution to migration. Similarly, invasion was significantly decreased but not prevented in Pten-rescued $TRP^{-/-}$ astrocytes; instead, rescued $TRP^{-/-}$ cells showed 58% and 32% reduction in invasion compared with control GFP-infected $TRP^{-/-}$ cells at 3 and 5 days, respectively ($P \leq .0003$) (Fig. 4E). These data are consistent with data in Fig. 3C, in which $TRP^{-/-}$ invasion was only partially mitigated after pharmacologically inhibiting PI3K or mTOR.

To confirm the Kras-independent effects of Pten on migration, we restored Pten in cells without activated Kras ($TP^{-/-}$). Wound closure was reduced to 7.6% (Supplementary Fig. S4), levels comparable to those in T astrocytes. This demonstrated that Pten loss significantly contributed to migration in the absence of Kras activation.

Activated MAPK and PI3K Signaling in G1/S-Defective Astrocytes Produces Gene Expression Profiles Similar to Human Proneural HGA

Results above demonstrate that the phenotypic effects of Kras activation and Pten loss are contextual and complementary. Next, we determined their effects on genome-wide transcriptome patterns using microarrays. These experiments showed that cultured G1/S-defective astrocytes display distinct expression profiles depending on the presence of activated Kras, Pten loss, or both. Consensus clustering of 23 samples identified 4 classes with high confidence (Supplementary Fig. S5); 3 of these classes (22 samples) were used in subsequent analyses (see Supplemental Methods). Although different isolates from identical genotypes were sometimes present in different clusters, Class 1 contained only T and TP astrocytes, Class 2 contained all analyzed TR astrocytes, and Class 3 contained only TRP astrocytes (Fig. 5A). Compared with Class 1 and 2, Class 3 (green bar) astrocyte transcriptomes were significantly enriched for migration, invasion, and stem cell signatures (Fig. 5B, Supplementary Table S1). These data are consistent with the above results demonstrating maximal migration and invasion in TRP astrocytes and suggest that these astrocytes may be stem-like and capable of initiating tumorigenesis.

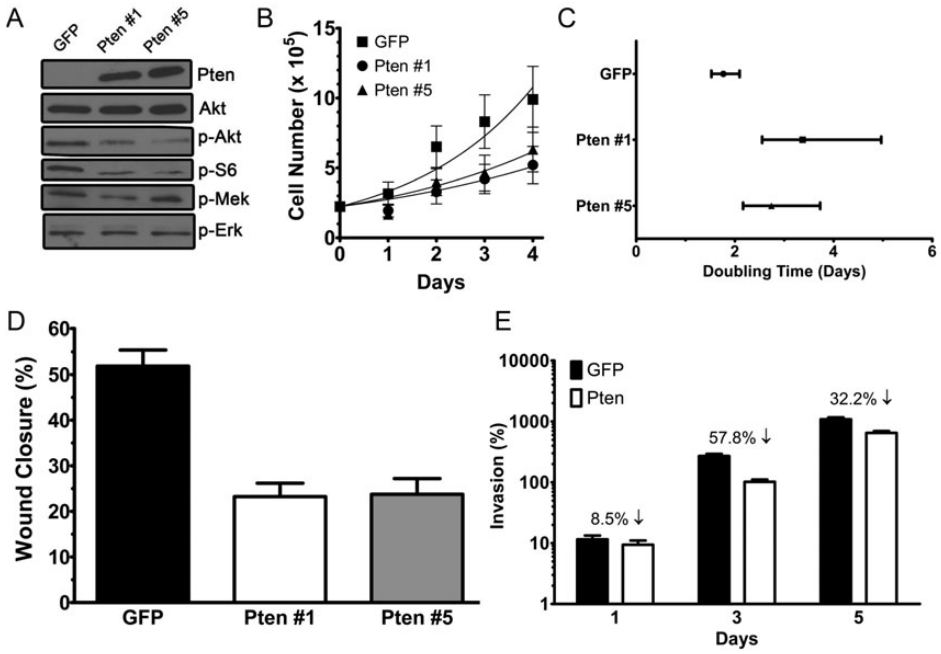

Fig. 4. Restoration of Pten expression limits growth, migration, and invasion in $TRP^{-/-}$ astrocytes. Representative immunoblot of MAPK and PI3K pathway signaling in $TRP^{-/-}$ astrocytes after infection with retrovirus containing Pten or GFP cDNA (A). Growth (B), doubling time (C), mean percent wound closure at 24 h (D), and mean percent invasion into collagen at 1, 3, and 5 days (E) of Pten rescued versus nonrescued (GFP) $TRP^{-/-}$ astrocytes. Mean doubling times $\pm$ 95% confidence intervals in C were calculated from the exponential growth curves in B. All experiments are the mean of at least three independent experiments using different astrocyte isolations. Error bars are SEM.

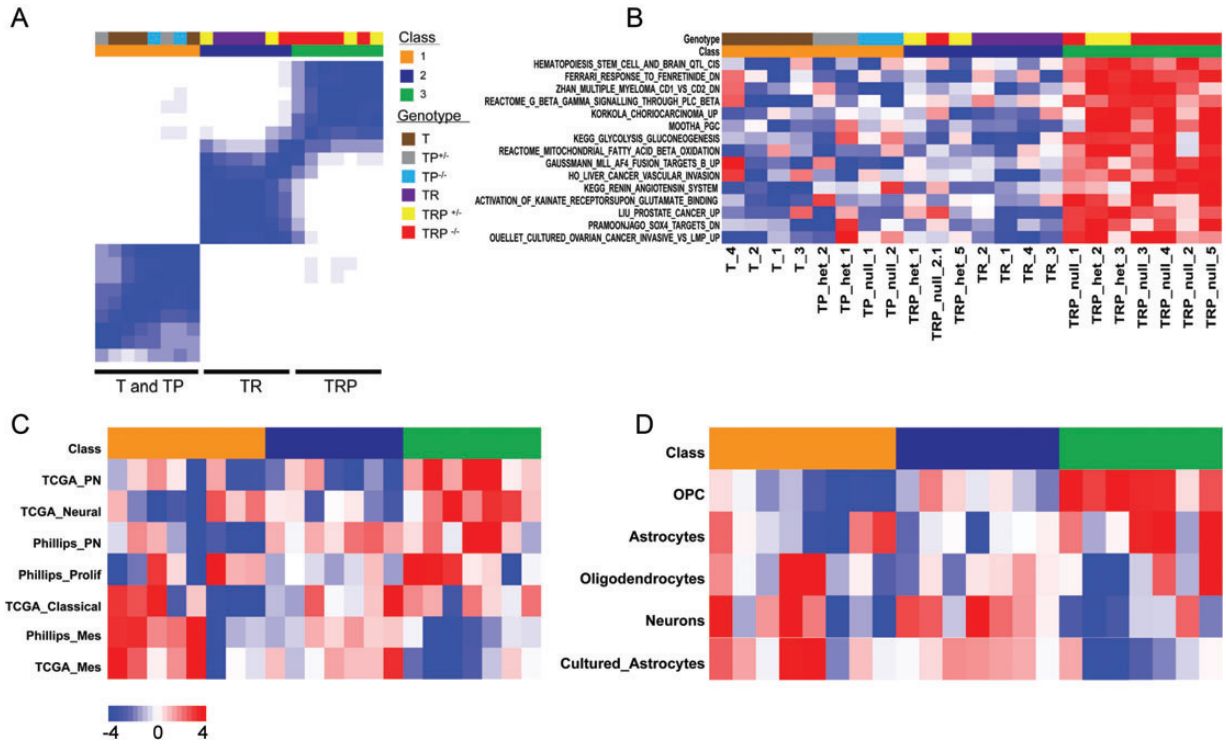

Fig. 5. Gene expression profiling of G1/S-defective astrocytes with activated Kras and/or *Pten* deletion. Consensus clustering of 22 independently isolated astrocyte cultures identifies 3 clusters (A). Individual isolates are repeated on the X and Y axes. Darker shades of blue signify isolates that cluster together most often. Single sample GSEA (ssGSEA) of the 15 most significantly enriched gene signatures from MsigDB in Class 3 (green) astrocytes (B). ssGSEA of human GBM signatures (C). ssGSEA of murine neural lineage signatures (D). Red signifies higher enrichment scores of signature genes.

Next, we examined whether these astrocytes were enriched for TCGA human GBM[26] and Phillips prognostic HGA[27] subtype signatures using gene set analysis (GSA) (Supplementary Table S2) and single sample gene set enrichment analysis (ssGSEA) (Fig. 5C). Class 3 TRP astrocytes were highly enriched for TCGA proneural and neural signatures ($P \leq .003$) and showed particularly low expression of the TCGA ($P = .09$) and Philips ($P = .04$) mesenchymal subtype signatures. Individual Class 3 astrocytes were also enriched for Phillips proneural and proliferative signatures, but the entire group was not significantly associated with them ($P \geq .1$). None of the HGA signatures were significantly enriched in Class 1 T/TP or Class 2 TR astrocytes, but several samples in these classes expressed low levels of proneural and neural signatures, further highlighting their dissimilarity to Class 3 TRP astrocytes.

We then investigated expression of adult murine neural cell lineage-specific signatures.[28] Class 3 TRP astrocytes showed high expression of oligodendrocyte progenitor (OPC)-specific genes and low expression of cultured astrocytes-specific genes (Fig. 5D, Supplementary Table S2), suggesting that the combination of Kras activation and Pten loss induces a more primitive expression pattern in G1/S-defective astrocytes. In contrast, Class 1 (T, TP) astrocytes showed low expression of OPC signature genes but instead expressed cultured astrocyte-specific genes.

A PI3K Activation Signature Is Enriched in Human Proneural GBM

Because PI3K signaling activation caused by Pten loss was critical for proliferation, migration, and invasion of G1/S-defective $TRP^{-/-}$ astrocytes, we next defined gene signatures specific to activated PI3K signaling. First, PI3K signaling was pharmacologically inhibited in $TRP^{-/-}$ astrocytes using the dual PI3K/mTOR inhibitor PI-103, the PI3K inhibitor LY294002, and the mTOR inhibitor rapamycin. Each drug maximally inhibited Akt-mediated S6 phosphorylation within 2–4 h of treatment, and maximal inhibition lasted at least 24 h, except LY2940 02, which lasted 4 h (Supplementary Fig. S6A–D). To identify PI3K pathway signatures, we analyzed mRNA expression of drug-treated samples after 4 h of inhibition (inhibited) and 4, 8, and 24 h after release from inhibition (released). We used large average submatrices (LAS), an unsupervised significance-based biclustering method, to identify groups of coordinately expressed genes.[29]

The top 5 biclusters, in order of decreasing statistical significance, consisted of genes highly expressed in the following contexts (data not shown): (i) all times after LY294002 release; (ii) all inhibited samples, regardless of the specific drug; (iii) 24 h after release from inhibition, regardless of the drug; (iv) all times after rapamycin release; and (v) all times after PI-103 release. The fifth bicluster of genes highly expressed after PI-103 release was selected as the PI3K signature for further investigation (Supplementary Table S3). The first bicluster was excluded because the relatively high concentration of LY294002 (50 μm) required to produce maximal inhibition of PI3K signaling showed slightly reduced viability relative to untreated $TRP^{-/-}$ cells at 24 h (93% ± 2%, data not shown), was likely to produce off-target effects, and was less efficient than PI-103 in inhibiting Akt phosphorylation (Supplementary Fig. S6D). The second was excluded because we sought to identify genes that defined activated, not inhibited PI3K signaling. The third was excluded because genes expressed only after 24 h of drug release would not contain genes expressed at earlier time points. The fourth was excluded because rapamycin-mediated inhibition of mTOR complex 1 (mTORC1) ablated S6, but not Akt phosphorylation (Supplementary Fig. S6C). Consequently, genes expressed after rapamcyin release would represent only a distal PI3K pathway activation signature. In contrast, PI-103 inhibits PI3K and both mTOR complexes, and it efficiently reduced phosphorylation of both Akt and S6 in $TRP^{-/-}$ astrocytes (Supplementary Fig. S6A). Furthermore, Akt and S6 phosphorylation increased after PI-103 release, suggesting that both proximal and distal PI3K pathway signaling resumed in $TRP^{-/-}$ astrocytes released from PI-103 (Supplementary Fig. S6A, D, E). We identified 518 genes (Supplementary Table S3) with increased expression after PI-103 release as a PI3K pathway activation signature and found that these genes clustered G1/S-defective $TRP^{-/-}$ astrocytes on the basis of inhibition or release from each individual drug (Fig. 6A).

Expression of PI3K signature genes was next examined in 434 human GBM from TCGA[30] and was significantly different across the 4 subtypes (Fig. 6B). Proneural GBM, in particular, showed significantly higher expression of PI3K signature genes by ssGSEA (Fig. 6C).

Kras Activation with or without Pten Loss Is Necessary for G1/S-Defective Astrocyte Tumorigenesis

The complimentary effects of Kras activation and Pten loss produced highly proliferative, migratory, and invasive G1/S-defective astrocytes in vitro, and their gene expression profiles correlated with human HGA subtypes. Next, we used an allograft model system with syngeneic, immunocompetent hosts to investigate whether Kras activation and/or Pten loss was required for tumorigenesis in vivo. Orthotopic injection of T, TR, $TRP^{+/-}$, and $TRP^{-/-}$ astrocytes produced astrocytomas in 30%, 25%, 64%, and 60% of mice aged up to 1 year or neurological morbidity (Fig. 7A). Three mice injected with T astrocytes developed small foci of LGA that failed to produce neurological symptoms and progress to HGA over the course of a year (Supplementary Fig. S7A–D). Four of 6 astrocytoma-bearing mice injected with TR astrocytes developed GBM (Supplementary Fig. 7B and S7E-H). Thus, although Kras activation was sufficient for malignant progression, TR GBM developed with long latency because median survival was 207 days (Fig. 7C). In contrast, G1/S-defective astrocytes containing both activated Kras and *Pten* deletion progressed to HGA in >97% of mice injected with either $TRP^{+/-}$ or

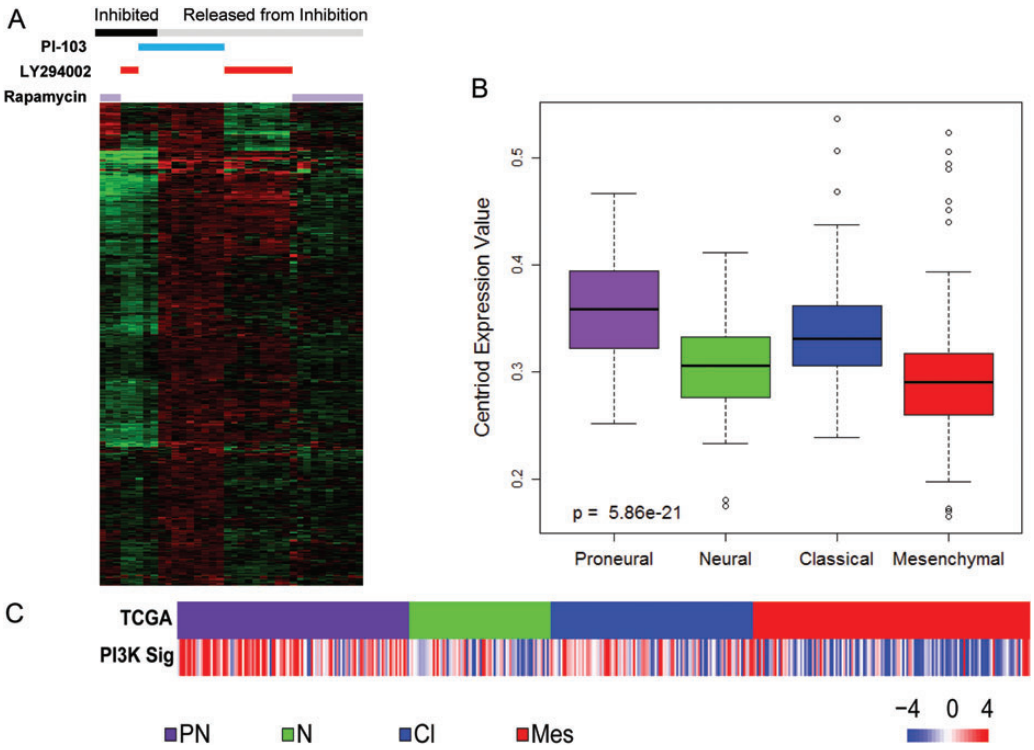

Fig. 6. A PI3K signature defined in TRP$^{-/-}$ astrocytes upon release from PI-103-mediated inhibition of PI3K signaling is enriched in human proneural GBM. Heatmap of 518 genes with significantly increased expression in TRP$^{-/-}$ astrocytes after release from PI-103 (A). A box and whiskers plot of the distribution of mean expression of PI3K signature genes (centroid) (B) and ssGSEA (C) shows that the PI3K signature is significantly enriched in human proneural (PN), but not neural (N), classical (Cl), and mesenchymal (Mes) GBM from TCGA.

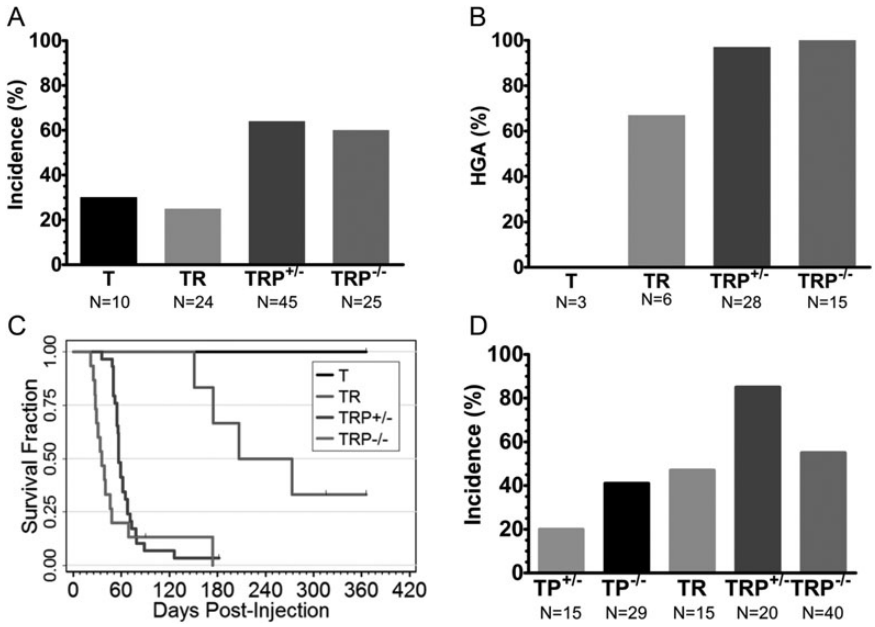

Fig. 7. G1/S-defective astrocytes form astrocytomas after orthotopic injection into syngeneic, immunocompetent mouse brains. Astrocytoma incidence in terminally aged mice after orthotopic injection of 10^5 astrocytes (A). The number of mice injected per genotype is indicated. The fraction of astrocytomas in panel A with histological features of high-grade astrocytomas (HGA) (B). The number of astrocytomas detected per genotype is indicated. Kaplan–Meier survival analysis of astrocytoma-bearing mice (C). Median survivals were 36, 57, and 207 days for TRP$^{-/-}$, TRP$^{+/-}$, and TR astrocytes, respectively ($P < .0001$). The incidence of astrocytomas in mice sacrificed between 7 and 28 days after injection with astrocytes of the indicated genotypes (D).

$TRP^{-/-}$ astrocytes, and 89% and 83% of these mice developed GBM, respectively (Fig. 7B, Supplementary Fig. S7I-P). *Pten* deletion also significantly decreased the latency of G1/S-defective, Kras-activated HGA because the median survival of mice injected with $TRP^{+/-}$ and $TRP^{-/-}$ astrocytes was 57 and 36 days, respectively ($P \leq .005$) (Fig. 7C). These results show that ablation of the G1/S checkpoint is sufficient to produce LGA, Kras activation is required for progression to HGA, and the combination of Kras activation and *Pten* deletion dramatically increases GBM incidence and reduces survival.

TRP (Supplementary Fig. S7IJ and S7MN) were significantly more invasive than TR GBM (Supplementary Fig. S7EF), which largely developed as well-circumscribed masses. These findings are consistent with the increased invasion of TRP versus TR astrocytes in vitro (Fig. 3B). Moreover, TRP GBM contained cells with both astrocytic and oligodendroglial morphology (Supplementary Fig. S7L and S7P), a finding consistent with their proneural GBM and murine OPC-like gene expression profiles in vitro.

To further examine tumor initiation, we injected G1/S-defective astrocytes with (TR, $TRP^{+/-}$, and $TRP^{-/-}$) and without ($TP^{+/-}$ and $TP^{-/-}$) activated Kras, sacrificed mice every 7 days for 4 weeks, and evaluated tumor incidence and histological grade. Similar to T astrocytes, $TP^{+/-}$ and $TP^{-/-}$ astrocytes infrequently developed into LGA (Fig. 7D and Supplementary Fig. S8). In contrast, $TRP^{+/-}$ and $TRP^{-/-}$ astrocytes developed into LGA more efficiently. Mitotically active HGA were evident in 40% and 10% of mice injected with these cells, but only one mouse injected with $TRP^{-/-}$ astrocytes developed a GBM within 28 days. These results suggest that the increased incidence of HGA in mice injected with TRP astrocytes is likely to be attributable to more efficient tumor initiation.

Discussion

Virtually all human GBM contain RB pathway gene mutations that dysregulate the G1/S cell cycle checkpoint. Most also contain RTK pathway gene mutations that activate RAS/MAPK and PI3K signaling.[4] We therefore used G1/S checkpoint-defective cortical murine astrocytes to examine the individual and combined effects of Ras/MAPK and/or PI3K pathway dysregulation on multiple cancer-related phenotypes in vitro. Both Kras activation and Pten loss induced MAPK and PI3K signaling (Fig. 1). Kras activation, but not Pten loss, increased proliferation and reduced apoptosis of cultured T^{+}_{121} astrocytes in vitro (Fig. 1D). We have previously shown that T_{121} induces both proliferation and apoptosis in neonatal, T_{121}-driven astrocytomas in vivo and that Pten loss potentiates progression by reducing apoptosis.[21] These findings suggest that Kras and Pten signaling perturbations may affect G1/S-defective astrocyte growth by distinct mechanisms depending on their patterns of co-occurrence. The role of Pten in p53-dependent apoptosis has long been recognized, but increasing evidence suggests that nuclear Pten directly regulates mitosis.[31] Decreasing Pten induces expression of cell cycle and chromosome stability genes and proliferation of mouse embryonic fibroblasts.[32] Moreover, *Pten* deletion in embryonic mice increases astrocyte proliferation in vitro and in vivo.[33] Conversely, exogenous PTEN expression in human glioma cells decreases proliferation and lengthens cell cycle transit from G2/M to G1.[34] Therefore, we conclude that Pten negatively regulates proliferation in G1/S-defective astrocytes.

Kras activation and/or *Pten* deletion not only increased MAPK and PI3K pathway signaling and growth of G1/S-defective astrocytes (Fig. 1) but migration as well (Fig. 2). However, their effects on invasion were contextual (Fig. 3). Kras activation was insufficient for invasion in the absence of *Pten* deletion, suggesting that Ras-mediated invasion requires concurrent activation of PI3K signaling. In contrast, monoallelic *Pten* deletion was sufficient to induce maximal invasion only in the presence of activated Kras (Fig. 3B). Biallelic *Pten* deletion caused maximal invasion in both the presence and the absence of activated Kras (Fig. 3B), and Pten restoration significantly reduced invasion (Fig. 4E). However, Pten restoration did not completely abrogate migration and invasion, likely because of $<100\%$ transfection efficiency. Thus, a subpopulation of cells in these assays lacked Pten expression and retained their migratory and invasive properties. These results indicate that Pten is a primary regulator of G1/S-defective astrocyte invasion and that the invasion-related effects of biallelic, but not monoallelic, *Pten* deletion are independent of activated Kras.

Established human cell lines, such as U87MG, have previously been used in genetic gain and loss of function studies to investigate the molecular mechanisms of GBM migration and invasion in vitro.[35] PTEN restoration has been shown to inhibit proliferation, migration, and invasion of human *PTEN*-null U87MG astrocytoma cells in vitro.[36] PDGF-induced migration of U87MG cells has also been shown to be PI3K, but not ERK, dependent,[37] and farnesyltransferase-mediated inhibition of Ras reduced U87MG migration in a PI3K-dependent manner.[38] However, established cell lines harbor widespread genomic alterations that frequently differ from their original tumor.[39,40] Therefore, panels of established cell lines, each with distinct genomic landscapes, are typically used to rule out cell line-specific effects. Our use of an allelic series of genetically defined astrocytes containing defined core signaling pathway mutations removes ambiguity associated with established human cell lines and provides a unique opportunity to clarify genotype-phenotype relationships in GBM pathogenesis. Our data therefore confirm and extend studies that used established human astrocytoma cell lines to demonstrate that PTEN is a critical regulator of migration and invasion and that RAS-dependent invasion requires PI3K/PTEN signaling.

In addition to their effects on growth, migration, and invasion, mutations that activate Ras/MAPK and PI3K signaling produced 3 distinct gene expression clusters that correlated with mutation and pathway activation status (Fig. 5). Activation of both pathways in cultured TRP astrocytes defined a transcriptomal class (Class 3) enriched for migratory, invasive, and stem-like signatures.

TRP astrocytes also showed high expression of human proneural GBM and murine OPC signatures. These findings are consistent with previous reports demonstrating similarity between proneural GBM and OPC.[26,28] Additionally, an activated PI3K pathway signature defined in TRP astrocytes released from PI3K pathway inhibition was enriched in human proneural GBM (Fig. 6).

The above data suggest that TRP astrocytes would form invasive astrocytomas in vivo. We used a novel orthotopic allograft model with syngeneic, immunocompetent hosts to show that G1/S-defective astrocytes with activated Kras and/or *Pten* deletion formed astrocytomas with penetrance that correlated with mutational status (Fig. 7). Specifically, both Kras activation and *Pten* deletion were required for high-penetrance tumorigenesis and efficient progression to HGA. Similar results were obtained in conditional, inducible GEM, in which these genetic mutations are targeted specifically to adult GFAP+ cortical astrocytes.[20] These findings suggest that cortical astrocytes may serve as a potential astrocytoma cell of origin, particularly in tumors with G1/S checkpoint dysfunction, activated Kras, and *Pten* deletion.

TRP allografts diffusely invaded normal brain and formed histopathological hallmarks of human astrocytomas, including perineuronal and perivascular sattelitosis, migration and invasion along white matter tracks, elevated mitoses, microvascular proliferation, and necrosis (Supplementary Fig. S7). These histopathological features contrast significantly with human U87MG GBM xenografts, which are poorly invasive in vivo,[23] and suggest that this model system will be useful for further dissection of the genetics of astrocytoma migration and invasion. We conclude that the syngeneic, orthotopic TRP allograft model represents a significant improvement over traditional xenografts models that use established human cell lines and immunodeficient mice.

Consistent with the expression profiles of TRP astrocytes in vitro (Fig. 5) and the presence of oligodendroglial differentiation in vivo (Supplementary Fig. S7), TRP allografts also showed enriched expression of human proneural GBM and murine OPC signature genes (manuscript in preparation). The Rb family of G1/S cell cycle proteins, Nf1, a negative regulator of Ras/MAPK signaling, and Pten have each been shown to regulate neural stem cell self-renewal and fate.[41–43] These results suggest that combined dysregulation of Rb, Ras, and Pten reverts astrocytes to a progenitor-like state of gene expression.

The use of gene expression profiling to characterize the molecular heterogeneity and improve diagnostic classification of specific types of brain tumors has recently brought significant attention to defining their cellular origins. We used GEM models to show that the molecular heterogeneity of medulloblastoma, the most common primary brain tumor in children, has a cellular and genetic basis.[44] Similar to HGA, multiple genomic subtypes of human medulloblastoma with distinct mutations exist.[45] Furthermore, GEM models have shown that different initiating oncogenic mutations in specific cells of origin in the developing mouse cerebellum lead to distinct genomic subtypes of medulloblastoma that mimic their human counterparts.

Gene expression profiling of human HGA has suggested that the subtypes may have distinct cellular origins.[26,46] GEM modeling studies have identified neural stem cells[47] and OPC[46] as potential candidate astrocytoma cells of origin.[48] PDGF-driven murine GBM derived from adult *Pten*-null OPC were shown to have transcriptomes similar to human proneural GBM.[46] Here, we identified proneural and OPC-like expression specifically in G1/S-defective neonatal murine astrocytes with activated Kras and *Pten* deletion (Fig. 5D). The presence of human proneural GBM and OPC-like expression profiles in both PDGF-driven GBM and TRP astrocyte-derived GBM allografts suggests that molecularly similar GBM can arise from at least 2 distinct genetic mechanisms and cellular origins. We speculate that multiple cell types can lead to GBM and that different cells are uniquely susceptible, within defined developmental windows, to the transforming effects of particular combinations of core signaling pathway mutations. These combined factors determine the human astrocytoma transcriptomal subtype. Such a unifying hypothesis would explain the associations between transcriptomal subtype, mutational landscape, signaling pathway alterations, and neural signatures in human GBM.[26,27,49]

The in vitro experiments described above show that growth, motility, and invasive phenotypes are differentially affected by specific genetic alterations in the RTK core GBM-signaling pathway. These alterations may ultimately dictate targeted GBM therapy. As such, we have used MAPK- and PI3K-targeted drugs to reduce in vitro migration, invasion, and signaling in TRP astrocytes transcriptionally similar to human proneural GBM (Fig. 2D, 3C, Supplementary Fig. S6). Release of TRP astrocytes from pharmacological PI3K pathway inhibition identified a PI3K signature significantly enriched in human proneural GBM (Fig. 6). The findings that TRP astrocytes contained a PI3K activation signature enriched in proneural human GBM and produced proneural-like HGA allografts after injection into syngeneic, immunocompetent brains suggest that proneural GBM may be uniquely sensitive to combination therapies targeting both RAS/MAPK and PI3K. The TRP allograft model of human proneural GBM will not only facilitate delineation of the molecular requirements for tumorigenesis and cellular origins of astrocytomas but will also be useful for preclinical testing of drug combinations and elucidating potential mechanisms of resistance. Moreover, the use of syngeneic, immunocompetent hosts will facilitate preclinical testing of immunotherapies.

Supplementary Material

Supplementary material is available online at *Neuro-Oncology* (http://neuro-oncology.oxfordjournals.org/).

Funding

NOK was supported by a postdoctoral fellowship from the American Cancer Society (PF-06-283-01-MGO). CRM is

a Damon Runyon-Genentech Clinical Investigator supported in part by a Clinical Investigator Award from the Damon Runyon Cancer Research Foundation (CI-45-09). This work was supported in part by grants to CRM from the UNC University Cancer Research Fund (UCRF) and the Department of Defense (W81XWH-09-2-0042). The UNC TPL is supported, in part, by grants from the National Cancer Institute (3P30CA016086), National Institute of Environmental Health Sciences (3P30ES010126), Department of Defense (W81XWH-09-2-0042), and UCRF.

Conflict of interest. The authors declare no conflicts of interest.

Acknowledgments

We thank Lauren Huey and Daniel Roth for technical assistance; Debbie Little, Mervi Eeva, and Stephanie Cohen for assistance with histology, immunohistochemistry, and digital image analysis; Robert Bagnell and the UNC Microscopy Services Laboratory for microscopy assistance; Serguei Kozlov for provision of plasmids; and Pablo Tamayo for ssGSEA R scripts. Portions of this work were presented at the 2012 annual meetings of the American Association for Cancer Research, American Association of Neuropathologists, and Society for Neuro-oncology. Author contribution for this work includes: conception and design: MV, NOK, TVD, and CRM; development of methodology: MV, NOK, REB, AMW, RSS, and CRM; acquisition of data: MV, NOK, REB, AMW, RSS, KKW, RSM, and SW; analysis and interpretation of data: MV, NOK, RSS, RSM, BH, and CRM; writing, review, and/or revision of the manuscript: MV and CRM; administrative, technical, or material support: TVD and CRM; study supervision: CRM.

References

1. CBTRUS. CBTRUS Statistical Report: Primary Brain and Central Nervous System Tumors Diagnosed in the United States in 2004-2008. Hinsdale, IL: Central Brain Tumor Registry of the United States; 2012.
2. Gaspar LE, Fisher BJ, Macdonald DR, et al. Supratentorial malignant glioma: patterns of recurrence and implications for external beam local treatment. *Int J Radiat Oncol Biol Phys*. 1992;24:55–57.
3. Giese A, Bjerkvig R, Berens ME, Westphal M. Cost of migration: invasion of malignant gliomas and implications for treatment. *J Clin Oncol*. 2003;21:1624–1636.
4. TCGA. Comprehensive genomic characterization defines human glioblastoma genes and core pathways. *Nature*. 2008;455:1061–1068.
5. Workman P, Clarke PA, Raynaud FI, van Montfort RL. Drugging the PI3 kinome: from chemical tools to drugs in the clinic. *Cancer Res*. 2010;70:2146–2157.
6. Jeuken J, van den Broecke C, Gijsen S, Boots-Sprenger S, Wesseling P. RAS/RAF pathway activation in gliomas: the result of copy number gains rather than activating mutations. *Acta Neuropathol*. 2007;114:121–133.
7. Guha A, Feldkamp MM, Lau N, Boss G, Pawson A. Proliferation of human malignant astrocytomas is dependent on Ras activation. *Oncogene*. 1997;15:2755–2765.
8. Reardon DA, Rich JN, Friedman HS, Bigner DD. Recent advances in the treatment of malignant astrocytoma. *J Clin Oncol*. 2006;24:1253–1265.
9. Ohgaki H, Kleihues P. Genetic pathways to primary and secondary glioblastoma. *Am J Pathol*. 2007;170:1445–1453.
10. Snuderl M, Fazlollahi L, Le LP, et al. Mosaic amplification of multiple receptor tyrosine kinase genes in glioblastoma. *Cancer Cell*. 2011;20:810–817.
11. Jun HJ, Acquaviva J, Chi D, et al. Acquired MET expression confers resistance to EGFR inhibition in a mouse model of glioblastoma multiforme. *Oncogene*. 2012;31:3039–3050.
12. Mellinghoff IK, Wang MY, Vivanco I, et al. Molecular determinants of the response of glioblastomas to EGFR kinase inhibitors. *N Engl J Med*. 2005;353:2012–2024.
13. Di Cristofano A, Pesce B, Cordon-Cardo C, Pandolfi PP. Pten is essential for embryonic development and tumour suppression. *Nat Genet*. 1998;19:348–355.
14. Suzuki A, de la Pompa JL, Stambolic V, et al. High cancer susceptibility and embryonic lethality associated with mutation of the PTEN tumor suppressor gene in mice. *Curr Biol*. 1998;8:1169–1178.
15. Di Cristofano A, Pandolfi PP. The multiple roles of PTEN in tumor suppression. *Cell*. 2000;100:387–390.
16. Parsons DW, Jones S, Zhang X, et al. An integrated genomic analysis of human glioblastoma multiforme. *Science*. 2008;321:1807–1812.
17. Xiao A, Wu H, Pandolfi PP, Louis DN, Van Dyke T. Astrocyte inactivation of the pRb pathway predisposes mice to malignant astrocytoma development that is accelerated by PTEN mutation. *Cancer Cell*. 2002;1:157–168.
18. Dannenberg JH, van Rossum A, Schuijff L, te Riele H. Ablation of the retinoblastoma gene family deregulates G(1) control causing immortalization and increased cell turnover under growth-restricting conditions. *Genes Dev*. 2000;14:3051–3064.
19. Jackson EL, Willis N, Mercer K, et al. Analysis of lung tumor initiation and progression using conditional expression of oncogenic K-ras. *Genes Dev*. 2001;15:3243–3248.
20. Miller CR, Karpinich NO, Zhang Q, Bullitt E, Kozlov S, Van Dyke T. Modeling astrocytomas in a family of inducible genetically engineered mice:implications for preclinical cancer drug development. In: Van Meir, EG, ed. CNS cancer: Models, markers, prognostic factors, targets, and therapeutic approaches. Dordrecht: Humana; 2009:119–140.
21. Xiao A, Yin C, Yang C, Di Cristofano A, Pandolfi PP, Van Dyke T. Somatic induction of Pten loss in a preclinical astrocytoma model reveals major roles in disease progression and avenues for target discovery and validation. *Cancer Res*. 2005;65:5172–5180.
22. Stec DE, Davisson RL, Haskell RE, Davidson BL, Sigmund CD. Efficient liver-specific deletion of a floxed human angiotensinogen transgene by adenoviral delivery of Cre recombinase in vivo. *J Biol Chem*. 1999;274:21285–21290.
23. Miller CR, Williams CR, Buchsbaum DJ, Gillespie GY. Intratumoral 5-fluorouracil produced by cytosine deaminase/5-fluorocytosine gene therapy is effective for experimental human glioblastomas. *Cancer Res*. 2002;62:773–780.
24. Rodriguez LG, Wu X, Guan JL. Wound-healing assay. *Methods Mol Biol*. 2005;294:23–29.

25. Smalley KS, Haass NK, Brafford PA, Lioni M, Flaherty KT, Herlyn M. Multiple signaling pathways must be targeted to overcome drug resistance in cell lines derived from melanoma metastases. *Mol Cancer Ther*. 2006;5:1136–1144.
26. Verhaak RG, Hoadley KA, Purdom E, et al. Integrated genomic analysis identifies clinically relevant subtypes of glioblastoma characterized by abnormalities in PDGFRA, IDH1, EGFR, and NF1. *Cancer Cell*. 2010;17:98–110.
27. Phillips HS, Kharbanda S, Chen R, et al. Molecular subclasses of high-grade glioma predict prognosis, delineate a pattern of disease progression, and resemble stages in neurogenesis. *Cancer Cell*. 2006;9:157–173.
28. Cahoy JD, Emery B, Kaushal A, et al. A transcriptome database for astrocytes, neurons, and oligodendrocytes: a new resource for understanding brain development and function. *J Neurosci*. 2008;28:264–278.
29. Shabalin AA, Weigman VJ, Perou CM, Nobel AB. Finding large average submatricies in high dimensional data. *Ann Appl Stat*. 2009;3:985–1012.
30. Cerami E, Gao J, Dogrusoz U, et al. The cBio cancer genomics portal: an open platform for exploring multidimensional cancer genomics data. *Cancer Discov*. 2012;2:401–404.
31. Planchon SM, Waite KA, Eng C. The nuclear affairs of PTEN. *J Cell Sci*. 2008;121:249–253.
32. Alimonti A, Carracedo A, Clohessy JG, et al. Subtle variations in Pten dose determine cancer susceptibility. *Nat Genet*. 2010;42:454–458.
33. Fraser MM, Zhu X, Kwon CH, Uhlmann EJ, Gutmann DH, Baker SJ. Pten loss causes hypertrophy and increased proliferation of astrocytes in vivo. *Cancer Res*. 2004;64:7773–7779.
34. Inaba N, Kimura M, Fujioka K, et al. The effect of PTEN on proliferation and drug- and radiosensitivity in malignant glioma cells. *Anticancer Res*. 2011;31:1653–1658.
35. Demuth T, Berens ME. Molecular mechanisms of glioma cell migration and invasion. *J Neurooncol*. 2004;70:217–228.
36. Li Y, Guessous F, DiPierro C, et al. Interactions between PTEN and the c-Met pathway in glioblastoma and implications for therapy. *Mol Cancer Ther*. 2009;8:376–385.
37. Cattaneo MG, Gentilini D, Vicentini LM. Deregulated human glioma cell motility: inhibitory effect of somatostatin. *Mol Cell Endocrinol*. 2006;256:34–39.
38. Goldberg L, Kloog Y. A Ras inhibitor tilts the balance between Rac and Rho and blocks phosphatidylinositol 3-kinase-dependent glioblastoma cell migration. *Cancer Res*. 2006;66:11709–11717.
39. Clark MJ, Homer N, O'Connor BD, et al. U87MG decoded: the genomic sequence of a cytogenetically aberrant human cancer cell line. *PLoS Genet*. 2010;6:e1000832.
40. Li A, Walling J, Kotliarov Y, et al. Genomic changes and gene expression profiles reveal that established glioma cell lines are poorly representative of primary human gliomas. *Mol Cancer Res*. 2008;6:21–30.
41. Jori FP, Galderisi U, Napolitano MA, et al. RB and RB2/P130 genes cooperate with extrinsic signals to promote differentiation of rat neural stem cells. *Mol Cell Neurosci*. 2007;34:299–309.
42. Gregorian C, Nakashima J, Le Belle J, et al. Pten deletion in adult neural stem/progenitor cells enhances constitutive neurogenesis. *J Neurosci*. 2009;29:1874–1886.
43. Dasgupta B, Gutmann DH. Neurofibromin regulates neural stem cell proliferation, survival, and astroglial differentiation in vitro and in vivo. *J Neurosci*. 2005;25:5584–5594.
44. Pei Y, Moore CE, Wang J, et al. An animal model of MYC-driven medulloblastoma. *Cancer Cell*. 2012;21:155–167.
45. Northcott PA, Korshunov A, Pfister SM, Taylor MD. The clinical implications of medulloblastoma subgroups. *Nat Rev Neurol*. 2012;8:340–351.
46. Lei L, Sonabend AM, Guarnieri P, et al. Glioblastoma models reveal the connection between adult glial progenitors and the proneural phenotype. *PLoS One*. 2011;6:e20041.
47. Alcantara Llaguno S, Chen J, Kwon CH, et al. Malignant astrocytomas originate from neural stem/progenitor cells in a somatic tumor suppressor mouse model. *Cancer Cell*. 2009;15:45–56.
48. Schmid RS, Vitucci M, Miller CR. Genetically engineered mouse models of diffuse gliomas. *Brain Res Bull*. 2012;88:72–79.
49. Brennan C, Momota H, Hambardzumyan D, et al. Glioblastoma subclasses can be defined by activity among signal transduction pathways and associated genomic alterations. *PLoS One*. 2009;4:e7752.